



Repositorio Institucional de la Universidad Autónoma de Madrid

<https://repositorio.uam.es>

Esta es la **versión de autor** del artículo publicado en:

This is an **author produced version** of a paper published in:

Advanced Functional Materials 26.33 (2016): 6060-6068

DOI: <http://dx.doi.org/10.1002/adfm.201601953>

Copyright: © 2016 WILEY-VCH Verlag GmbH & Co. KGaA, Weinheim

El acceso a la versión del editor puede requerir la suscripción del recurso

Access to the published version may require subscription

DOI: 10.1002/ ((please add manuscript number))

Article type: Full paper

Infrared-emitting QDs for thermal therapy with real time subcutaneous temperature feedback

*Blanca del Rosal, Elisa Carrasco, Fuqiang Ren, Antonio Benayas, Fiorenzo Vetrone ,
Francisco Sanz-Rodríguez, Dongling Ma, Ángeles Juarranz de la Fuente, and Daniel Jaque**

B. del Rosal, Francisco Sanz-Rodríguez Dr. D. Jaque
Fluorescence Imaging Group, Departamento de Física de Materiales, Facultad de Ciencias,
Universidad Autónoma de Madrid, Madrid 28049, Spain.
E-mail: daniel.jaque@uam.es

Dr. E. Carrasco
Instituto de Investigaciones Biomédicas “Alberto Sols”, CSIC-UAM, Madrid 28029, Spain.

Dr. E. Carrasco, Prof. A. Juarranz de la Fuente
Grupo de Dermatología Experimental, Instituto Ramón y Cajal de Investigación Sanitaria,
IRYCIS, Madrid 28034, Spain

F. Ren, Dr. A. Benayas, Dr. F. Vetrone, Dr. D. Ma
Institut National de la Recherche Scientifique Centre – Énergie Matériaux et
Télécommunications, Université du Québec, Varennes, QC J3X 1S2, Canada

Dr. F. Vetrone
Centre for Self-Assembled Chemical Structures, McGill University, Montréal, QC, H3A 2K6,
Canada

Dr. D. Jaque and Francisco Sanz-Rodríguez
Instituto Ramón y Cajal de Investigación Sanitaria, IRYCIS, Hospital Ramón y Cajal, 28034
Madrid, Spain

Keywords: Quantum dots, photothermal therapy, infrared imaging, nanothermometry

Nowadays, one of the most exciting applications of nanotechnology in biomedicine is the development of localized, non-invasive therapies for diverse diseases, such as cancer. Among them, nanoparticle-based photothermal therapy (PTT), which destroys malignant cells by delivering heat upon optical excitation of nanoprobes injected into a living specimen, is emerging with great potential. Two main milestones that must be reached for PTT to become a viable clinical treatment are deep penetration of the triggering optical excitation, and real-time accurate temperature monitoring of the ongoing therapy, which constitutes a critical factor to minimize collateral damage. In this work, an as of yet unexplored capability of near-infrared emitting semiconductor nanocrystals (QDs) is demonstrated. Here, temperature self-monitored QD-based PTT is presented for the first time using PbS/CdS/ZnS QDs emitting in the second biological window. These QDs are capable of acting, simultaneously, as photothermal agents (heaters) and high-resolution fluorescent thermal sensors, making it possible to achieve full control over the intratumoral temperature increment during PTT. The differences observed between intratumoral and surface temperatures in this comprehensive investigation, through different irradiation conditions, highlight the need for real-time control of the intratumoral temperature that allows for a dynamic adjustment of the treatment conditions in order to maximize the efficacy of the therapy.

1. Introduction

The recent development of nanotechnology has brought about significant advances in the biomedical field.^[1] A great variety of nanoparticles (NPs) with different functionalities, including imaging, temperature sensing, drug delivery or therapy have been fabricated and applied successfully at both the cellular and small animal level.^[2] One of the therapeutic applications of NPs is thermal therapy of cancer, which consists in the destruction of malignant tumors by subjecting them to high temperatures for a certain amount of time.^[3] Although magnetic NPs, which release heat upon application of an alternating magnetic field, have been explored as thermal therapeutic agents for a long time,^[4] photothermal NPs, capable of light-induced heating, have been much less investigated yet have attracted increasing interest in the past few years.^[5] The greatest limitation of photothermal therapy (PTT) lies in the penetration depth of light into tissues, which makes it impossible to treat deeply embedded tumors in a minimally invasive manner without resorting to endoscopy techniques.^[6] The penetration depth of light into tissues is maximum for wavelengths lying in the spectral ranges known as the biological windows (BWs), which correspond to the following ranges: 700-950 nm (first BW, BW-I), 1000-1350 nm (second BW, BW-II) and 1500-1800 nm (third BW, BW-III).^[7] In these spectral windows, absorption and scattering of light by tissues is minimum, which allows for penetration depths greater than 1 centimeter.^[8] Wavelengths in the BWs, being scarcely absorbed by the tissues, will result in a minimum energy deposition and therefore, in a reduced non-selective light-induced damage.^[8b, 9] The majority of NPs that have been successfully used as photothermal agents for therapy in animal models are optically excited within the first BW, typically with 808 nm radiation.^[5a] This particular wavelength has been found optimum for developing accurate thermal therapies based on cost-effective commercial lasers.

Among all the photothermal NPs used up to now, gold nanostructures are the most extensively explored, thanks to their excellent light-to-heat conversion efficiencies.^[10]

However, other NPs, including carbon nanotubes,^[11] graphene NPs,^[12] and neodymium-doped NPs,¹³ ^[13] also present a remarkable photothermal conversion efficiency and, additionally, provide a near-infrared (NIR) fluorescence signal which can be used to track the location of the NPs inside the body. Furthermore, fluorescent NPs can provide additional functionalities, such as intratumoral temperature sensing. This is the case, for instance, of neodymium-doped LaF₃ NPs, whose emission band shape is temperature-dependent.^[14] The possibility of heating and sensing temperature under excitation with a single laser beam is extremely interesting, as temperature constitutes a key parameter that needs to be carefully controlled during PTT in order to ensure the complete destruction of the cancer cells while causing minimum damage to surrounding healthy tissues. Even under identical irradiation conditions, parameters such as the number and distribution of NPs and more importantly, the vascular environment of the tumor, which varies significantly depending on the tumor characteristics, will affect the laser-induced temperature increment.^[15] As a consequence, the use of different numerical models and calculations not based on experimental observations could lead to wrong estimations of intratumoral temperature increments and, hence, cannot be used to design the parameters of the therapy.

Most reports concerning thermally controlled PTTs use thermographic imaging as a means to monitor the temperature during the treatment.^[16] However, this technique only allows detection of the surface temperature (sometimes referred to as apparent temperature), which may be significantly different from that at the tumor site, as has been demonstrated in previous works.^[14, 17] Moreover, changes in the tissue emissivity during the treatment would affect the measurement, leading to a suboptimal temperature control. Consequently, more accurate tools are required for measuring the intratumoral temperature, which could be effectively achieved if the NPs used as photothermal agents could double as in situ thermometers. This possibility has been demonstrated by Zhu et al. using core/shell NPs with a fluorescent temperature-sensitive core and a photothermal carbon shell.^[17] However, two

different laser wavelengths (730 and 980 nm, this last causing non-selective heating of tissues) are required for simultaneously exciting the luminescence and the heat production. This not only complicates the experimental setup, but also causes uncertainty about the thermal reading as the penetration depths of both excitation wavelengths into the irradiated tissue are not equal.

Semiconductor quantum dots (QDs) have been extensively explored for in vitro applications thanks to their outstanding properties, including bright fluorescence emission signals, size-based tunability and demonstrated biocompatibility.^[18] However their use as fluorescent probes for deep tissue imaging in animal models has been somewhat limited.^[18-19] This is due to the fact that most of them absorb and emit in the visible range of the spectrum, thus being of little use for performing high penetration in vivo imaging. However, a variety of NIR-emitting QDs have been synthesized in the past few years and have recently emerged as very promising in vivo contrast agents particularly in that they can be used at very low concentrations and excitation power densities, further minimizing any potential toxicity. These QDs are capable of in vivo anatomical fluorescence imaging, and thus provide the possibility of performing in vivo biodistribution studies and monitoring tumor therapy processes, as has been recently demonstrated.^[9a, 20]

Among the different NIR-emitting QDs, PbS/CdS/ZnS QDs have been tested for deep tissue imaging in a mouse model with remarkable success. Although a long-term study concerning the effects of Cd-based QDs in non-human primates reported minimal toxicity 90 days after injection,^[21] toxicity always constitutes a concern when seeking NPs for biological applications. PbS/CdS/ZnS QDs, with a robust outer ZnS shell that results in a complete isolation of the PbS core and CdS inner shell from the environment, have been demonstrated to be biocompatible by previously carried out in vitro and in vivo toxicity studies.^[20a] Not only are these QDs high-brightness fluorescent probes in BW-II, but they are also capable of temperature sensing, as the intensity of the emission band, centered at around 1270 nm,

decreases linearly with increasing temperature. Based on their thermal sensitivity, PbS/CdS/ZnS QDs have already been postulated as attractive candidates for temperature monitoring during deep tissue PTT. It is clear that these QDs are effective in delivering a diagnostic modality (imaging, nanothermometry, etc.) yet no therapeutic modality has been demonstrated with only the QDs. In the case that they possessed, light-to-heat conversion capabilities, they would emerge as extremely interesting candidates for PTT with intratumoral temperature control. Their dual character as photothermal agents and fluorescent thermometers in the second biological window could also be of interest for other applications besides photothermal therapy of tumors, such as thermal non-contact stimulation of brain activities with real temperature feedback.^[22] Nevertheless, the possibility of activating light-to-heat conversion processes in PbS/CdS/ZnS QDs has not been investigated yet.

In this work, we explored PbS/CdS/ZnS QDs as efficient infrared photothermal agents by taking advantage of the nonradiative de-excitations that are activated after electronic excitation with an 808 nm laser beam. The simultaneous generation of a temperature-sensitive fluorescence signal (due to interband radiative de-excitations) is investigated as a tool to provide real-time quantitative feedback and spatial distribution of the optically-induced temperature increase during the thermal therapy in each case. The use of infrared excited/infrared emitting PbS/CdS/ZnS QDs for fully controlled thermal therapy of tumors in mouse models has been systematically investigated and the advantages of PbS/CdS/ZnS for simultaneous thermal therapy, fluorescence imaging and thermometry over other photothermal agents and techniques have been discussed.

2. Results and discussion

The core/shell/shell PbS/CdS/ZnS QDs used in this work were synthesized by capping two different shells on the initial PbS QDs, as is described in detail in the Methods section. The QDs show an average diameter of 4 nm, as calculated from the analysis of TEM images, one

of which is included as an inset in **Figure 1**. The NIR emission spectrum of an aqueous dispersion of the QDs at different temperatures is represented in **Figure 1(a)**. In this figure, it can be clearly observed that the intensity of the emission band centered at around 1270 nm is strongly dependent on the QD temperature. Several heating and cooling cycles were performed in order to obtain the calibration curve represented in **Figure 1(b)**, where the normalized emission intensity is represented as a function of temperature. Temperature-induced quenching was found to be fully reversible, as no significant differences were observed between the recorded intensities during heating and cooling procedures. It was also found that repeated heating and cooling cycles did not produce any changes in the emission spectrum of the QDs, as can be seen in **Figure S1**, suggesting that the repeated heating did not affect their structural integrity. As can be observed in Figure 1(b), the emission intensity experiences a linear decrease with temperature. A linear fit of the experimental data can be performed in order to obtain the fluorescence thermal sensitivity of the QDs used in this work, S , which is defined as follows:

$$S = \frac{1}{I} \frac{dI}{dT} \quad (1)$$

where I corresponds to the emitted intensity and T to the temperature. From the slope of the linear fit represented in Figure 1(b), a thermal sensitivity of $10^{-2} \text{ }^{\circ}\text{C}^{-1}$ around room temperature has been determined. This value is among the highest fluorescence thermal sensitivities previously reported for other fluorescent nanothermometers, as can be seen in Table S1 in the Supporting Information. From the data in table S1, it is clear that the fluorescent probes which clearly beat the PbS/CdS/ZnS QDs as temperature sensors, such as the widely used Er^{3+} , Yb^{3+} -doped NPs, present absorption or emission bands in the visible range of the spectrum, thus being unsuitable for in vivo applications.

When compared to other NIR-absorbing and emitting fluorescent probes which present a temperature-sensitive emission, such as Nd^{3+} -doped NPs, PbS/CdS/ZnS QDs present several

additional advantages. These include a higher temperature sensitivity (by one order of magnitude) and an intense fluorescence signal, which ensures that even at low QD concentrations or irradiation power densities, the temperature-sensitive signal will be easily detected with a conventional InGaAs NIR camera.^[20a] Furthermore, temperature reading with Nd-based nanothermometers requires, in addition, a more complex experimental setup, as it is based on temperature-induced spectral changes. Therefore, a spectral analysis of the emission signal in real time is required. PbS/CdS/ZnS QDs open the possibility of achieving real-time thermal feedback by using a single NIR camera without requiring the use any spectral filtering or analysis components.^[23]

When CdS/PbS/ZnS QDs are excited with an 808 nm laser, both radiative and nonradiative de-excitation processes are expected to happen, as is schematically represented in **Figure 2(a)**. Thus, the temperature-sensitive radiative emission (providing PbS/CdS/ZnS QDs with thermal sensitivity) is accompanied by nonradiative transitions. Thus, PbS/CdS/ZnS QDs are expected to partially convert the absorbed optical energy into phononic energy, which confers them heating capabilities. The possibility of taking advantage of the heating capability of QDs for photothermal therapy has, indeed, already been demonstrated with CdTe and CdSe QDs, which release heat under 671 nm excitation..^[24] More recently, WS₂ QDs have been applied on a synergistic PTT and radiotherapy treatment of tumors in a mouse model.^[25] However, the possibility of performing PTT has never been explored using infrared excited/infrared emitting QDs which would provide the remarkable advantages of higher penetration depths and autofluorescence-free imaging. The heating capability of 808 nm laser excited PbS/CdS/ZnS QDs was first tested in aqueous dispersion and ex vivo experiments, injecting PbS/CdS/ZnS QDs dispersed in PBS (phosphate buffer saline) into a tissue. The results of the ex vivo experiments are presented in **Figure 2(b)**. It can be seen that, for the highest laser power density of 3 W/cm², the tissue injected with QDs experiences a maximum temperature increment at the surface of the injection site close to 25 °C. On the other hand, the

temperature increment observed for the control sample, injected with an equivalent amount of PBS, has been found to be as low as 2 °C. This remarkable difference evidences a relevant light-to-heat conversion capability of PbS/CdS/ZnS QDs. In order to ensure that the photothermal heating did not affect the temperature sensing capabilities of the QDs, we monitored their infrared emission through two 4-minute-long cycles of 808 nm laser irradiation (2 W/cm²). Before and after each heating cycle, the laser power was reduced by two orders of magnitude, in order to observe the QD fluorescence without the presence of any appreciable heating. As can be seen in **Figure S2**, the emission intensity returns to the original (baseline) room temperature values after the laser heating cycle, indicating that the observed decrease in intensity during the photothermal procedure can be solely attributed to changes in temperature and not to any degradation (nor physical nor chemical) in the QD.

The photothermal conversion efficiency, defined as the fraction of the absorbed power that is transformed into heat, was calculated following the method described by Roper et al.^[26] The detailed calculations, which can be found in the Supporting Information (section S2), yielded a photothermal conversion efficiency value of 43 %. This value is not among the highest of those reported in the literature for photothermal NPs, which exceed 90 % for some gold nanostructures, as can be seen in Table S2 in the Supporting Information, where the photothermal conversion efficiencies of different NPs are listed. Nevertheless, the additional features presented by PbS/CdS/ZnS QDs with respect to other photothermal agents (temperature-sensitive fluorescence in the BW-II and high biocompatibility) make them extremely interesting candidates for in vivo PTT. Furthermore, these PbS/CdS/ZnS QDs are comparatively small in size for an all-in-one heating and nanothermometry platform. Unlike other PTT agents recently reported, -such as up-converting nanoparticles (UCNPs) linked to polypyrrole (PPy),^[27] PEGylated antimony nanorod bundles,^[28] or core/shell UNCNP/carbon nanocomposites,^[17] the QDs reported here keep are only a few nanometers in diameter, which makes them fully suitable for the desired biomedical application.

As mentioned before, the PbS/CdS/ZnS QDs used in this work have been reported to show little toxicity in in vitro experiments.^[20a] However, toxicity assays were here performed with QDs previously heated to 80 °C for 4 minutes, as well as with non-heated QDs, so as to check that their biocompatibility was not hampered by the heating procedure. The results are represented in **Figure S4**, indicating that the toxicity associated to the QDs at the cellular level is virtually identical for heated and non-heated QDs. This constitutes a strong evidence of the structural integrity of the QDs even after exposed to temperatures equal or higher than those reached during PTT, as any leakage of heavy metals would have resulted in a significant increase in toxicity.^[29]

In order to experimentally evaluate the application of PbS/CdS/ZnS QDs for temperature-controlled PTT of malignant tumors, a series of in vivo experiments, schematically represented in **Figure 3(a)** and **(b)** were designed and conducted. Briefly, the mice were subcutaneously inoculated with 3×10^6 A431 cells per flank to induce tumor growth. When the tumors reached a total volume of around 100 mm³, they were subjected to study. The treated tumors were subcutaneously injected with 60 µL of a dispersion of QDs in PBS at a concentration of 5 mg/mL, whereas the tumors used as laser only control cases were injected with 60 µL of pure PBS solution. Both treated and laser-only control tumors were then irradiated a single time with an 808 nm laser diode for 4 minutes, which is a suitable duration for a photothermal treatment if ablation temperatures are reached. During this period, the emission of the QDs was continuously monitored with a NIR camera in order to ensure the localization of the QDs at the tumor site as well as to monitor the intratumoral temperature during the treatment. Simultaneously, the surface temperature was measured through thermographic imaging. Different irradiation power densities were used in order to determine the optimum irradiation doses leading to efficient and minimally invasive treatment. Also, this allowed us to evaluate the difference between the intratumoral and surface (skin) temperatures under various irradiation conditions.

The intratumoral fluorescence intensity generated by the injected QDs during the PTT decreases with time following an exponential trend, as is represented in **Figure 3(c)** for an irradiation power density of 1.7 W/cm^2 . Such a decrease in the fluorescence signal indicates, according to Figure 1(b), an increase in the intratumoral temperature. Other effects that could lead to intensity decreases (such as quenching due to intratumoral enzymatic metabolism, and gradual clearance of QDs from the tumor tissue) occur in the hour/day timescale, so that the observed intensity changes can be unequivocally attributed to temperature changes. This temperature-associated decrease in the intratumoral fluorescence is further evidenced in **Figure 3(f)** and **(g)**, which correspond to the fluorescence images recorded both at the beginning and at the end of the treatment. Additional evidence of the existence of relevant tumor heating during the PTT was obtained from the thermographic images obtained before and immediately after the PTT (**Figure 3(d)** and **(e)**, respectively). Both the fluorescence and thermographic images reveal the capacity of PbS/CdS/ZnS QDs to induce relevant tumor heating under 808 nm laser excitation.

From the fluorescence and thermographic images collected during the treatment, the time evolution of both intratumoral and surface temperatures can be obtained. Results obtained for an irradiation power density of 1.7 W/cm^2 are shown in **Figure 4(a)**. The first important conclusion that can be extracted from our measurements is that, although both intratumoral and surface temperatures show the same increasing trend with time, their actual values are markedly different. This observation is in agreement with previous works dealing with intratumoral temperature measurements during PTT, which reported a significant difference between both temperature values,^[14, 17] and also with numerical models dealing with temperature distribution in tissues undergoing hyperthermia therapy.^[30] This also makes the spatial and thermal accuracy of our thermal readout, based on the optically excited fluorescence of the injected QDs, much more reliable than other recent reports on PTT, all of them relying on thermographic imaging.^[25, 27-28] The difference between intratumoral and

surface temperatures has been systematically measured as a function of the irradiation density. Results are included in **Figure 4(b)**, in which the surface temperature increments induced in PBS + laser control tumors have been also included. Note that for all the excitation power densities investigated in this work, control temperature increments have been found to be significantly lower than the intratumoral heating induced by PbS/CdS/ZnS QDs. It is important to note at this point, however, that the observed temperature increment in the control case is much higher than that occurring in the ex vivo experiments; and also higher than that expected for nude mice under our irradiation conditions according to some previous reports.^[31] Nevertheless, literature concerning photothermal therapy under 808 nm laser irradiation in which the surface temperature was monitored using thermographic imaging report very different temperature increment values in the control experiments, as can be seen in detail in table S3 in the Supporting Information. These differences could be attributed to parameters that cannot be easily controlled, such as the vascular environment of the tumor to be treated. The same diversity of data in the literature is observed for the surface temperature in successful photothermal treatments, as can also be seen in Table S3. From the data included in Figure 4(b), it is also clear that the higher the irradiation power density, the greater the difference between superficial and intratumoral temperatures. These facts point out, once again, the need for a full control over the intratumoral temperature during PTT, not purely based on the surface temperature of the treated specimen, in such a way that the treatment conditions can be adjusted to each specific case.

Experimental data included in Figure 4(b) reveals that optically excited PbS/CdS/ZnS QDs can lead to intratumoral temperature increments as high as 45 °C, which should be enough to produce tumor regression. In order to evaluate this possible therapeutic effect, we systematically studied the post-treatment evolution of the tumors and determined the range of treatment conditions which resulted in successful therapy, as well as those who resulted in excessive or insufficient damage. The post-treatment observations are summarized in **Figure**

5. A representative image of a mouse in which a tumor had been generated in each flank, as obtained before the thermal therapy, is shown in **Figure 5(a)**. The evolution of a representative total control tumor and a treated tumor (1.7 W/cm^2) is shown in **Figure 5(b)**. It can be clearly seen that, while the control tumor experienced a significant growth, the treated one was completely ablated after the irradiation. The surface burn which appeared immediately after the irradiation was completely healed after three weeks, leaving behind nothing but a surface scar. The detailed evolution of the tumor size with time is displayed in **Figure 5(c)** (top) for the three different control conditions used in this work: tumors injected with pure PBS and subjected to laser irradiation (PBS + laser), non-irradiated tumors injected with QDs (QDs control) and non-injected non-irradiated tumors (total control). It can be observed that neither the QDs nor the laser irradiation alone have a therapeutic effect on eliminating or reducing the tumor. This fact points out that the intratumoral QD concentration used in our experiments does not inhibit the tumor growth at all. Even in the case of PBS + laser at the highest power density used in this work (2 W/cm^2), the tumor size 14 days after irradiation is four times that at the day of the procedure, although the growing trend of the tumor appeared to revert for a short period after the irradiation. The bottom graph corresponds to the tumors which were subjected to the full procedure, i.e, intratumoral QD injection + laser irradiation. It can be seen that the treatment at the lowest laser power densities (between 0.8 and 1.3 W/cm^2) had no therapeutic effect, as the tumor size kept increasing. We can therefore state that, for this range of irradiation power densities, we are producing insufficient heating and, hence, are unable of successfully ablating the tumors, as indicated in Figure 4(b) as “Insufficient heating”. However, irradiation densities between 1.7 and 2 W/cm^2 resulted in a complete destruction of the tumor and a full recovery of the treated mice after the skin wound generated as a consequence of the photothermal therapy was healed. Consequently, this range has been defined as the therapeutic range in Figure 4(b). Higher irradiation power densities (above 2 W/cm^2) led to excessive damage in the treated mice and, as discussed

earlier, even affected the growth of the PBS + laser control tumor. For such high power densities, we state that significant nonselective damage is taking place (range indicated as “Excessive damage” in Figure 4(b)). Three different regimes can be identified considering the post-treatment evolution of the tumors and the real time intratumoral temperature measurements:

- i) *Insufficient heating regime.*- Power densities below 1.5 W/cm^2 and intratumoral temperature increments below $35 \text{ }^\circ\text{C}$ do not lead to any relevant tumor regression.
- ii) *Successful tumor therapy regime.*- Power densities between 1.5 and 2.3 W/cm^2 that lead to intratumoral temperature increments between 35 and $50 \text{ }^\circ\text{C}$, which resulting efficient thermal therapy with minimal collateral effects. In this regime, the observed surface temperature increment is close to $25 \text{ }^\circ\text{C}$, which corresponds to a skin temperature of $55 \text{ }^\circ\text{C}$ at the end of the 4-minute-long treatment, as seen in Figure 3(d). Previous works dealing with PTT report similar surface temperature increments in successful tumor ablation in animal models (see Table S3 in Supporting Information).
- iii) *Excessive damage regime.*- Laser power densities of 2.3 W/cm^2 and higher lead to intratumoral temperature increments well above $50 \text{ }^\circ\text{C}$ that finally result in a substantial collateral damage in the treated tumor and even extensive skin damage in the PBS + laser control mouse.

Thus, data included in Figures 4 and 5 do not only constitute the first demonstration of the potential use of infrared-emitting QDs as photothermal therapeutic agents. In addition, they provide the intratumoral temperature ranges in which highly efficient photothermal treatment of malignant tumors is possible, being this between 30 and $50 \text{ }^\circ\text{C}$.

3. Conclusion

In this work, we present for the first time infrared-emitting PbS/CdS/ZnS QDs as therapeutic agents for photothermal treatment of malignant tumors. We have successfully demonstrated the possibility of tumor ablation in mice models which were intratumorally injected with QDs and subjected to 808 nm laser irradiation. Moreover, what makes these QDs particularly interesting for therapy is their temperature-sensitive fluorescence signal, which allows for continuously monitoring the intratumoral temperature variation during the photothermal treatment using just an NIR-sensitive camera. The excitation at 808 nm grants a low absorption of the excitation beam by animal tissues, which minimizes the undesired heating on healthy tissue volumes. The fact that the intense emission band of these QDs lies beyond 1200 nm not only allows a high penetration of the fluorescence signal into tissues, but also offers the possibility of autofluorescence-free imaging and thermal sensing. It is here demonstrated how these QDs make it possible to fully monitor and control the temperature at the tumor site during in vivo PTT of cancer tumors using a single excitation beam at 808 nm. Combination of intratumoral temperature measurements during treatment and post-treatment tumor evolution studies has allowed us to unequivocally identify the intratumoral temperature increments that ensure efficient therapy while avoiding excessive heating that causes undesired extensive skin damage during therapy.

Results included in this work open a new avenue towards the use of QDs for dynamically adjusted and minimally invasive photothermal treatments with real time intratumoral thermal feedback. This constitutes a great improvement with respect to the extensively used approaches based on infrared thermographic imaging, which provides thermal readings at the surface of the tumors which, as is here demonstrated, can differ significantly from the intratumoral temperature.

4. Experimental Section

Synthesis of PbS/CdS/ZnS QDs: Lead chloride (98%), sulfur (100%), oleylamine (OLA) (technical grade, 70%), cadmium oxide (99%), methanol (anhydrous, 99.8%), octadecene (ODE), mercaptopropyl acid (MPA) ($\geq 99.0\%$), 1-methyl-2-pyrrolidinone (NMP) ($\geq 99\%$), butylamine (99.5%), phosphorous pentasulfide (99%) and zinc chloride (99.999%) were obtained from Sigma-Aldrich Inc. Hexane, phosphate buffered saline (PBS, pH 7.4), oleic acid (OA), toluene, and ethanol were purchased from Fisher Scientific Company. All chemicals were used as purchased.

PbS QDs were synthesized by using OLA as capping ligands.^[32] In a typical reaction, 10 g of lead chloride and 24 mL of OLA were mixed and heated by oil bath to 160 °C and kept at this temperature for 1 h under the protection of N₂. The solution was then cooled to 120 °C and pumped for 30 min. The solution of 115 mg sulfur in 4 mL of OLA at room temperature was quickly injected into the PbCl₂-OLA suspension under vigorous stirring. The reaction cell was quenched with cold water after the reaction was conducted at 100 °C for 10 min to obtain PbS QDs.

PbS/CdS core shell QDs were synthesized following our previously reported method.^[33] Basically, 3 g of cadmium oxide, 15 mL of OA and 20 mL of ODE were heated in a separate flask to 200-250 °C using an oil bath until the solution turned colorless. The solution was cooled to 100 °C and degassed under vacuum for 30 min. The temperature was further decreased to 20 °C and 12 mL of PbS QD dispersion was added via syringe. Then 20 mL of this mixture solution was introduced into a 35 mL reaction tube, and then reacted in a microwave reactor (Discover; CEM Corporation) at 100 °C for 3 minutes.

PbS/CdS/ZnS core/shell/shell QDs with MPA as the capping ligand were prepared following our very recently developed procedure.^[20a] In a typical reaction, 0.045 mmol phosphorous pentasulfide, 0.4 mL MPA and 0.3 mL butylamine were heated at 110 °C for 20 minutes in 10 mL NMP in a sealed vial to dissolve the sulfide. In a separate vial, 0.51 mmol zinc chloride, 0.4 mL MPA and 0.3 mL butylamine were mixed in 10 mL NMP and heated to dissolve zinc

chloride in the same way. After cooling down to room temperature, 0.007 g of OLA-capped PbS/CdS QDs were dispersed in the phosphorous pentasulfide solution, and then mixed with the zinc chloride solution. The mixture was heated at 70 °C for 30 minutes, yielding the MPA-capped PbS/CdS/ZnS core/shell/shell QDs.

Spectroscopic characterization: the emission spectra were obtained upon excitation with a fiber-coupled 808 nm laser diode (Lumics) focused in a 100 μm deep microchannel (Ibidi) filled with the aqueous dispersion of QDs. In order to study the temperature dependence of the emission, the microchannel was placed on a Peltier-cooled temperature control stage (Linkam PE120). The fluorescence signal was collected by an InGaAs CCD camera (Andor iDus DU490A) after passing through appropriate filters and being spectrally analyzed by an Andor Shamrock 193i spectrometer.

Fluorescence and thermal imaging: All fluorescence images were collected using an InGaAs CCD camera with enhanced sensitivity in the 1000-1700 nm spectral range (XEva1.7-320). Optical excitation was achieved using a fiber-coupled 808 nm laser diode (LIMO) with a maximum output power of 10 W. A long pass filter with cut-off wavelength at 850 nm (Thorlabs FEL850) was used to remove the 808 nm pump background. Thermal images were recorded using a thermographic camera (FLIR E40bx).

Animal experiments: Seven female 8-weeks-aged athymic nude mice purchased from Envigo (France) were used for this study. Briefly, the mice were subcutaneously inoculated with 3×10^6 A431 cells per flank to induce tumor growth. When the tumors reached a total volume of at least 100 mm^3 , they were subjected to study. The treated tumors were subcutaneously injected with 60 μL (approximately half of the tumor volume) of a dispersion of QDs in PBS at a concentration of 5 mg/mL , whereas the tumors used as laser only control cases were injected with 60 μL of pure PBS solution. Both treated and laser-only control tumors were then irradiated for 4 minutes with a fiber-coupled 808 nm laser diode (LIMO), whose spot size was set to a total area of 2 cm^2 . Thermographic imaging was used to continuously

monitor surface temperature, while the QD emission in the fully treated (QDs + laser) animals was recorded using the aforementioned infrared camera. All the experimental procedures with animals were carried out in compliance with the 2013/63/UE European guideline and were approved by the Ethics Committee from Universidad Autónoma de Madrid (CEIT) in the frame of the project FIS-MAT2013-47395-C4-1-R supported by the Spanish Ministerio de Economía y Competitividad.

Supporting Information

S1. Stability of PbS/CdS/ZnS QDs upon heating; S2. Comparison of fluorescent nanothermometers; S3. Ex vivo photothermal treatment; S4. Calculation of the photothermal conversion efficiency of PbS/CdS/ZnS QDs; S5. Comparison of photothermal conversion efficiencies of different nanoheaters; S6. In vitro toxicity of PbS/CdS/ZnS after heating; S7. Comparison of surface temperatures achieved in PTT experiments. Supporting Information is available from the Wiley Online Library or from the author.

Acknowledgements

This project has been supported by the Spanish Ministerio de Economía y Competitividad under project and MAT2013-47395-C4-1-R. B. del Rosal thanks Universidad Autónoma de Madrid for an FPI grant. F. Ren acknowledges scholarship support from the Fonds de recherche du Québec – Nature et technologies (FRQNT) under the Programme de Bourses d'Excellence (Merit Scholarship Program for Foreign Students). A. Benayas is thankful to the Canadian Institutes of Health Research and the Breast Cancer Society of Canada (CIHR-BCSC), for postdoctoral funding granted to him through an Eileen Iwanicki Fellowship in Breast Cancer Imaging. F. Vetrone is grateful to the Natural Sciences and Engineering Research Council (NSERC) of Canada, FRQNT and the Canada Foundation for Innovation (CFI) for supporting his research program. F. Vetrone also gratefully acknowledges the Fondation Sibylla Hesse. D. Ma is grateful for the financial support from NSERC, FRQNT, CFI and the Centre Québécois sur les Matériaux Fonctionnels (CQMF), Canada.

Received: ((will be filled in by the editorial staff))

Revised: ((will be filled in by the editorial staff))

Published online: ((will be filled in by the editorial staff))

- [1] a) Q. Pankhurst, N. Thanh, S. Jones, J. Dobson, *J. Phys. D: Appl. Phys.* **2009**, *42*, 224001; b) E. C. Dreaden, A. M. Alkilany, X. Huang, C. J. Murphy, M. A. El-Sayed, *Chem. Soc. Rev.* **2012**, *41*, 2740; c) S. M. Janib, A. S. Moses, J. A. MacKay, *Adv. Drug Delivery Rev.* **2010**, *62*, 1052; d) G. Chen, H. Qiu, P. N. Prasad, X. Chen, *Chemical Reviews* **2014**, *114*, 5161.
- [2] a) P. Sharma, S. Brown, G. Walter, S. Santra, B. Moudgil, *Adv. Colloid Interface Sci.* **2006**, *123–126*, 471; b) M. A. Hahn, A. K. Singh, P. Sharma, S. C. Brown, B. M. Moudgil,

- Anal. Bioanal. Chem.* **2010**, 399, 3; c) F. Vetrone, R. Naccache, A. Zamarrón, A. Juarranz de la Fuente, F. Sanz-Rodríguez, L. Martínez Maestro, E. Martín Rodríguez, D. Jaque, J. García Solé, J. A. Capobianco, *ACS Nano* **2010**, 4, 3254; d) K. Cho, X. Wang, S. Nie, D. M. Shin, *Clinical cancer research* **2008**, 14, 1310; e) L. Zhang, F. Gu, J. Chan, A. Wang, R. Langer, O. Farokhzad, *Clinical pharmacology and therapeutics* **2008**, 83, 761; f) C. D. S. Brites, P. P. Lima, N. J. O. Silva, A. Millan, V. S. Amaral, F. Palacio, L. D. Carlos, *Nanoscale* **2012**, 4, 4799.
- [3] P. Wust, B. Hildebrandt, G. Sreenivasa, B. Rau, J. Gellermann, H. Riess, R. Felix, P. Schlag, *The Lancet Oncology* **2002**, 3, 487.
- [4] R. Hergt, S. Dutz, R. Müller, M. Zeisberger, *J. Phys.: Condens. Matter* **2006**, 18, S2919.
- [5] a) D. Jaque, L. Martínez Maestro, B. del Rosal, P. Haro-Gonzalez, A. Benayas, J. L. Plaza, E. Martín Rodríguez, J. García Solé, *Nanoscale* **2014**, 6, 9494; b) J. S. Donner, S. A. Thompson, C. Alonso-Ortega, J. Morales, L. G. Rico, S. I. C. O. Santos, R. Quidant, *ACS Nano* **2013**, 7, 8666.
- [6] J. A. Schwartz, A. M. Shetty, R. E. Price, R. J. Stafford, J. C. Wang, R. K. Uthamanthil, K. Pham, R. J. McNichols, C. L. Coleman, J. D. Payne, *Cancer Res.* **2009**, 69, 1659.
- [7] E. Hemmer, N. Venkatachalam, H. Hyodo, A. Hattori, Y. Ebina, H. Kishimoto, K. Soga, *Nanoscale* **2013**, 5, 11339.
- [8] a) S. Stolik, J. A. Delgado, A. Pérez, L. Anasagasti, *Journal of Photochemistry and Photobiology B: Biology* **2000**, 57, 90; b) A. M. Smith, M. C. Mancini, S. Nie, *Nat. Nanotechnol.* **2009**, 4, 710; c) A. Bashkatov, E. Genina, V. Kochubey, V. Tuchin, *J. Phys. D: Appl. Phys.* **2005**, 38, 2543.
- [9] a) G. Hong, J. T. Robinson, Y. Zhang, S. Diao, A. L. Antaris, Q. Wang, H. Dai, *Angew. Chem., Int. Ed.* **2012**, 51, 9818; b) T. Zako, M. Yoshimoto, H. Hyodo, H. Kishimoto, M. Ito, K. Kaneko, K. Soga, M. Maeda, *Biomaterials Science* **2015**, 3, 59.
- [10] a) X. Huang, I. H. El-Sayed, W. Qian, M. A. El-Sayed, *J. Am. Chem. Soc.* **2006**, 128, 2115; b) H. Kang, B. Jia, J. Li, D. Morrish, M. Gu, *Appl. Phys. Lett.* **2010**, 96, 063702.
- [11] J. T. Robinson, K. Welsher, S. M. Tabakman, S. P. Sherlock, H. Wang, R. Luong, H. Dai, *Nano Res.* **2010**, 3, 779.
- [12] K. Yang, S. Zhang, G. Zhang, X. Sun, S. T. Lee, Z. Liu, *Nano Lett.* **2010**, 10, 3318.
- [13] U. Rocha, K. Upendra Kumar, C. Jacinto, J. Ramiro, A. J. Caamaño, J. García Solé, D. Jaque, *Appl. Phys. Lett.* **2014**, 104, 053703.
- [14] E. Carrasco, B. del Rosal, F. Sanz-Rodríguez, Á. J. de la Fuente, P. H. Gonzalez, U. Rocha, K. U. Kumar, C. Jacinto, J. G. Solé, D. Jaque, *Adv. Funct. Mater.* **2015**, 25, 615.
- [15] C. W. Song, A. Lokshina, J. G. Rhee, M. Patten, S. H. Levitt, *Biomedical Engineering, IEEE Transactions on* **1984**, BME-31, 9.
- [16] S. C. Gnyawali, Y. Chen, F. Wu, K. E. Bartels, J. P. Wicksted, H. Liu, C. K. Sen, W. R. Chen, *Medical & biological engineering & computing* **2008**, 46, 159.
- [17] X. Zhu, W. Feng, J. Chang, Y.-W. Tan, J. Li, M. Chen, Y. Sun, F. Li, *Nat. Commun.* **2016**, 7.
- [18] A. L. Rogach, *Wien-New York: Springer* **2008**.
- [19] J. M. Klostranec, W. C. W. Chan, *Adv. Mater.* **2006**, 18, 1953.
- [20] a) A. Benayas, F. Ren, E. Carrasco, V. Marzal, B. del Rosal, B. A. Gonfa, Á. Juarranz, F. Sanz - Rodríguez, D. Jaque, J. García - Solé, *Adv. Funct. Mater.* **2015**, 25, 6650; b) A. L. Rogach, M. Ogris, *Current opinion in molecular therapeutics* **2010**, 12, 331.
- [21] L. Ye, K.-T. Yong, L. Liu, I. Roy, R. Hu, J. Zhu, H. Cai, W.-C. Law, J. Liu, K. Wang, J. Liu, Y. Liu, Y. Hu, X. Zhang, M. T. Swihart, P. N. Prasad, *Nat Nano* **2012**, 7, 453.

- [22] a) R. Chen, G. Romero, M. G. Christiansen, A. Mohr, P. Anikeeva, *Science* **2015**, 347, 1477; b) João L. Carvalho-de-Souza, Jeremy S. Treger, B. Dang, Stephen B. H. Kent, David R. Pepperberg, F. Bezanilla, *Neuron* **2015**, 86, 207.
- [23] a) A. Benayas, B. del Rosal, A. Pérez-Delgado, K. Santacruz-Gómez, D. Jaque, G. A. Hirata, F. Vetrone, *Adv. Opt. Mater.* **2015**, 3, 687; b) U. Rocha, C. Jacinto da Silva, W. Ferreira Silva, I. Guedes, A. Benayas, L. Martínez Maestro, M. Acosta Elias, E. Bovero, F. C. J. M. van Veggel, J. A. García Solé, D. Jaque, *ACS Nano* **2013**, 7, 1188; c) D. Wawrzynczyk, A. Bednarkiewicz, M. Nyk, W. Strek, M. Samoc, *Nanoscale* **2012**, 4, 6959.
- [24] M. Chu, X. Pan, D. Zhang, Q. Wu, J. Peng, W. Hai, *Biomaterials* **2012**, 33, 7071.
- [25] Y. Yong, X. Cheng, T. Bao, M. Zu, L. Yan, W. Yin, C. Ge, D. Wang, Z. Gu, Y. Zhao, *ACS Nano* **2015**, 9, 12451.
- [26] D. K. Roper, W. Ahn, M. Hoepfner, *The Journal of Physical Chemistry C* **2007**, 111, 3636.
- [27] X. Huang, B. Li, C. Peng, G. Song, Y. Peng, Z. Xiao, X. Liu, J. Yang, L. Yu, J. Hu, *Nanoscale* **2016**, 8, 1040.
- [28] W. Li, P. Rong, K. Yang, P. Huang, K. Sun, X. Chen, *Biomaterials* **2015**, 45, 18.
- [29] a) J. Lovrić, S. J. Cho, F. M. Winnik, D. Maysinger, *Chem. Biol.* **2005**, 12, 1227; b) Y. Su, Y. He, H. Lu, L. Sai, Q. Li, W. Li, L. Wang, P. Shen, Q. Huang, C. Fan, *Biomaterials* **2009**, 30, 19.
- [30] M. Jaunich, S. Raje, K. Kim, K. Mitra, Z. Guo, *Int. J. Heat Mass Transfer* **2008**, 51, 5511.
- [31] B. del Rosal, I. Villa, D. Jaque, F. Sanz-Rodríguez, *Journal of Biophotonics* **2015**, n/a.
- [32] L. Cademartiri, E. Montanari, G. Calestani, A. Migliori, A. Guagliardi, G. A. Ozin, *Journal of the American Chemical Society* **2006**, 128, 10337.
- [33] F. Ren, H. Zhao, F. Vetrone, D. Ma, *Nanoscale* **2013**, 5, 7800.

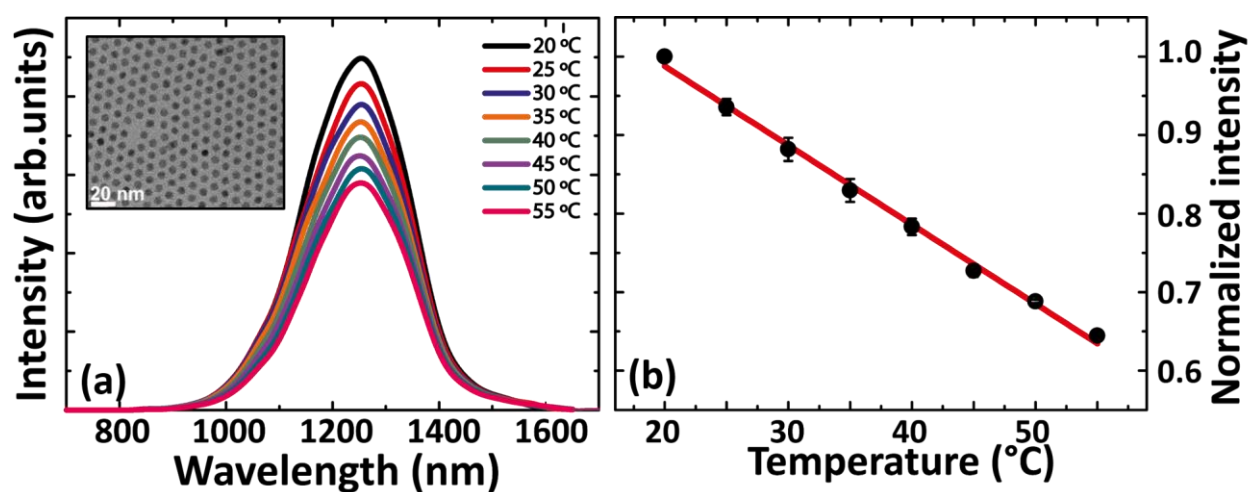


Figure 1. Characterization of PbS/CdS/ZnS QDs. (a) NIR emission spectra of an aqueous dispersion of the PbS/CdS/ZnS QDs used in this work at different temperatures. A representative TEM image of the QDs is given as an inset. (b) Emission intensity of the QD sample as a function of the temperature, normalized to its value at 20 °C. Dots correspond to the experimental data while line represents the best linear fit.

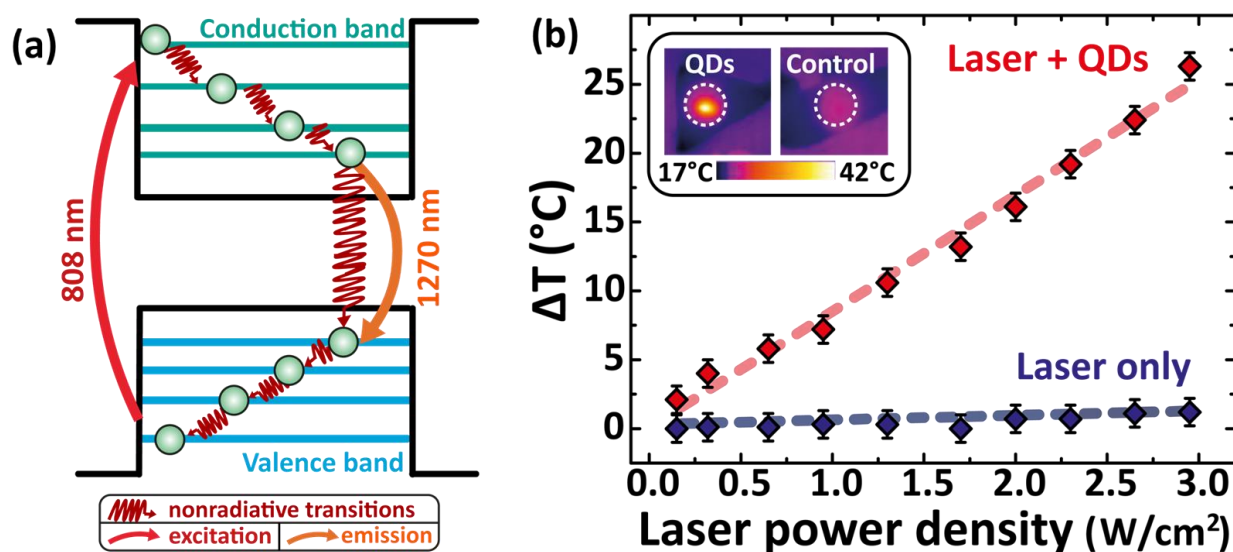


Figure 2. Photothermal effect in PbS/CdS/ZnS QDs. (a) Schematic representation of the energy levels of a PbS/CdS/ZnS QD, where the radiative and nonradiative transitions occurring after excitation with 808 nm radiation are indicated. (b) Ex vivo temperature increment of a tissue sample injected with QDs (red dots) or with the equivalent amount of PBS (blue dots) as a function of the 808 nm laser power density. The dashed lines are guides for the eyes. Thermographic images, such as the ones depicted in the inset, of the laser-irradiated tissue were used to evaluate the temperature increments for each laser power density.

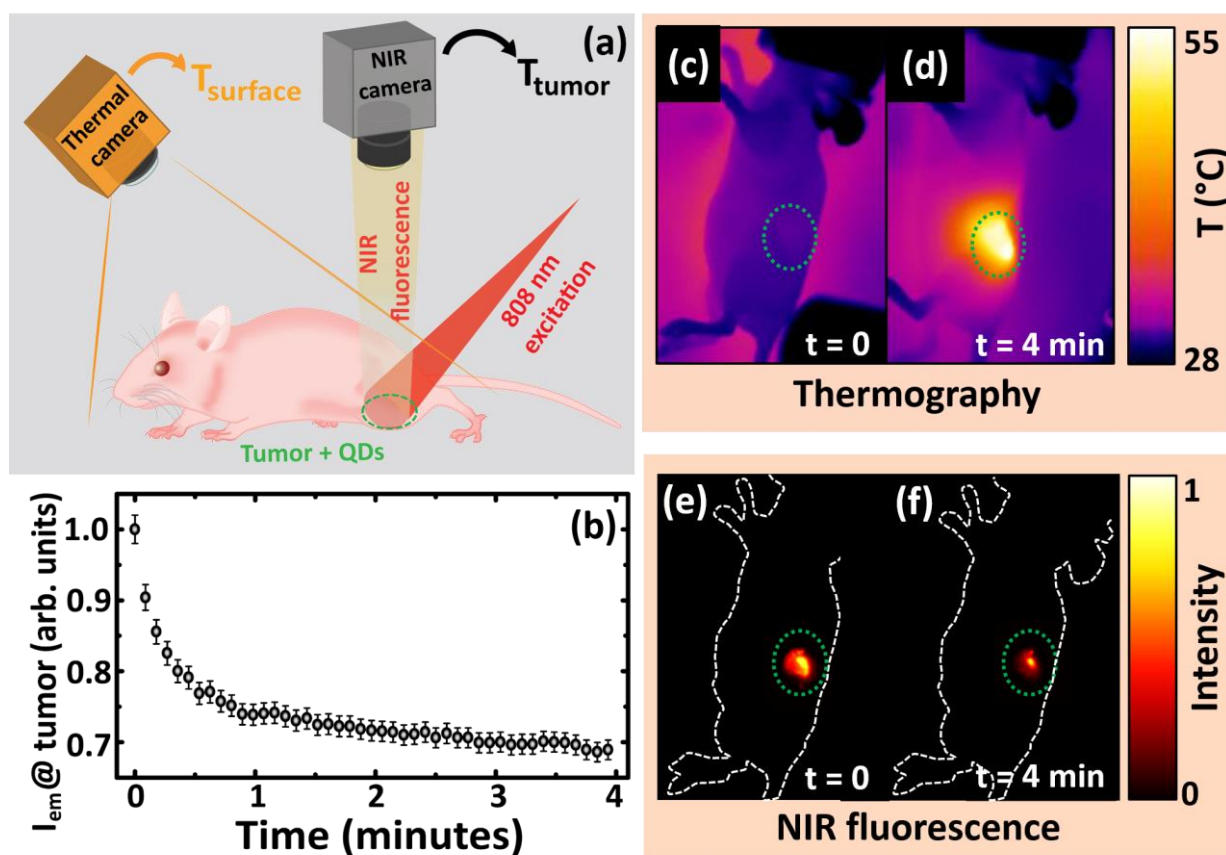


Figure 3. PTT with real-time temperature feedback. (a) Schematic representation of the treatment procedure: after intratumoral injection of 60 μL of a 5 mg/mL dispersion of PbS/CdS/ZnS QDs in PBS, the mice were irradiated with an 808 nm laser at different power densities, while the emission of the QDs was continuously monitored with an InGaAs camera. Additionally, the surface temperature was monitored during the procedure using a thermographic camera. (b) Time evolution of the emitted intensity of the intratumorally injected PbS/CdS/ZnS QDs during the treatment. (c)-(f) Thermographic and fluorescence images of the mouse treated with an 808 nm power density of 1.7 W/cm^2 before and at the end of the 4-minute-long irradiation. The location of the tumor injected with QDs is indicated in the four images with a dotted circle.

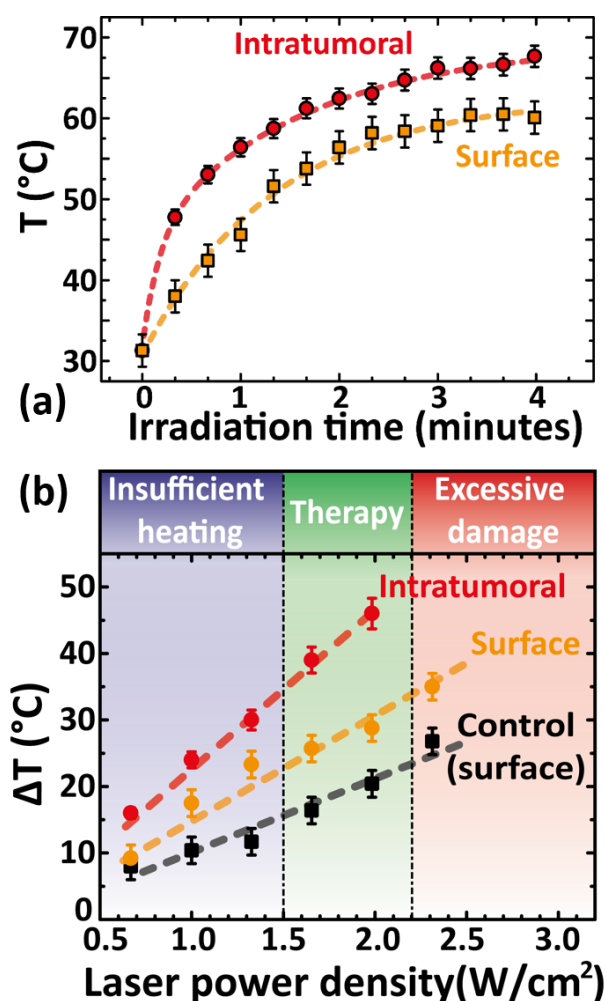


Figure 4. Temperature increment during treatment (a) Intratumoral temperature (red dots) and skin surface temperature (orange dots) measured during the photothermal treatment of a tumor under irradiation at $1.7 \text{ W}/\text{cm}^2$ with an 808 nm laser. The data were collected using the temperature-sensitive fluorescence of the QDs and a thermographic camera, respectively. The dashed lines represent guides for the eyes. (b) Temperature increment for different irradiation power densities measured at the tumor site (red dots) and at the skin surface (orange dots). The black dots represent the temperature increments at the tumor skin surface for control mice, which were injected with PBS. Three different ranges are indicated in the graph, which correspond to the different effects (no significant tumor damage, successful photothermal therapy and extensive damage to the tissues adjacent to the tumor) observed in the treated mice depending on the irradiation power density.

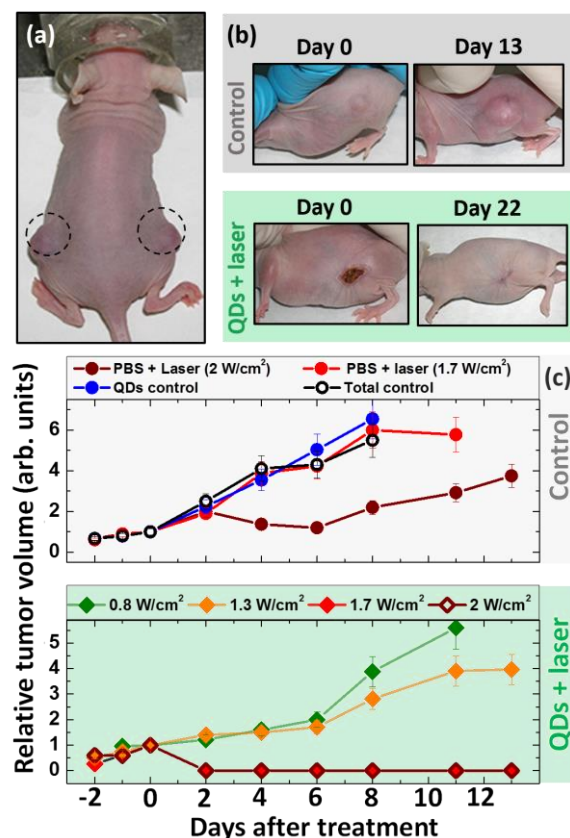
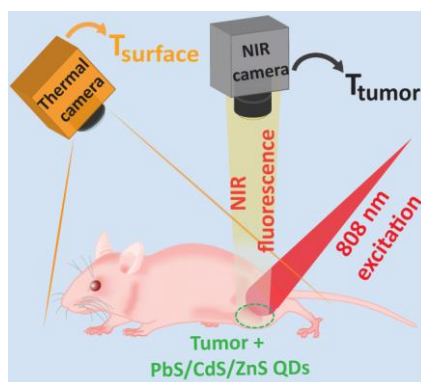


Figure 5. Evolution of the tumors after the treatment. (a) Representative mouse with one tumor in each flank (dashed circles), anaesthetized and ready for the treatment. (b) **Top:** Evolution of a total control tumor. **Bottom:** After the QDs + laser (1.7 W/cm²) treatment, the tumor dramatically disappeared and the wound produced as a consequence (left) was completely healed 22 days later (right). (c) **Top.** Size evolution of the tumors under different control conditions: total control (empty circles), QDs only (blue dots) and PBS + 808 nm laser at 1.7 and 2 W/cm² (red and brown dots, respectively). The dashed line indicates the day of the treatment. **Bottom.** Size evolution of the tumors treated with QDs and 808 nm laser irradiation at different power densities: 0.8 and 1.3 W/cm² (green and orange dots, respectively) did not prevent the tumor from further growing, while 1.7 and 2 W/cm² (red and brown dots, respectively) resulted in a complete destruction of the tumor. The dashed line indicates the day of the treatment. Error bars correspond to the uncertainty in the experimental determination of the tumor size ($\pm 15\%$).

PbS/CdS/ZnS QDs allow intratumoral temperature feedback in real time during photothermal therapy thanks to their temperature-sensitive fluorescence emission in the second biological window and remarkable photothermal conversion efficiency. A continuous monitoring of the intratumoral temperature, which differs greatly from that at the surface during the treatment makes possible a dynamic control of the therapy so as to maximize its efficacy.

Infrared-emitting QDs for thermal therapy with real time subcutaneous temperature feedback

B. del Rosal, E. Carrasco, F. Ren, A. Benayas, F. Vetrone, D. Ma, A. Juarranz de la Fuente and D. Jaque*



Supporting Information

Infrared-emitting QDs for thermal therapy with real time subcutaneous temperature feedback

*Blanca del Rosal, Elisa Carrasco, Fuqiang Ren, Antonio Benayas, Fiorenzo Vetrone, Dongling Ma, Ángeles Juarranz de la Fuente, and Daniel Jaque**

S1. Stability of PbS/CdS/ZnS QDs upon heating

The stability upon heating of the PbS/CdS/ZnS QDs was evaluated by subjecting an aqueous dispersion of the QDs to several 4-minute-long cycles of heating (up to 80 °C) and cooling. After each heating/cooling cycle, the infrared emission spectrum of the QDs under excitation with an 808 nm laser diode was collected. The emission spectra obtained before and after five heating cycles were virtually identical, as can be seen in **Figure S1**, suggesting that the repeated heating did not affect the structural integrity and properties of the QDs.

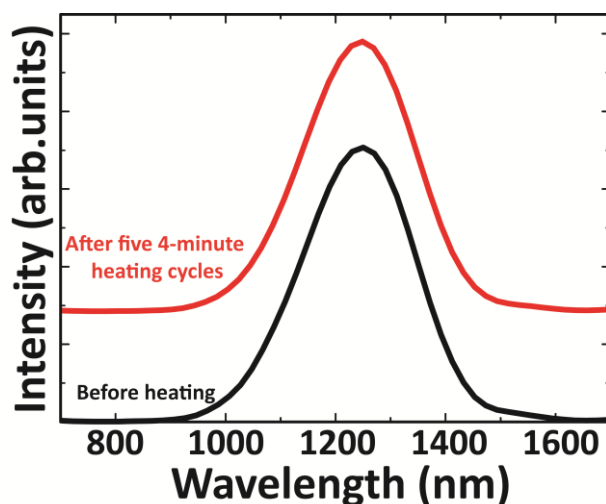


Figure S1. Emission spectrum of an aqueous solution of PbS/CdS/ZnS QDs under 808 nm excitation before and after being subjected to five 4-minute-long cycles of heating to 80 °C.

S2. Comparison of fluorescent nanothermometers

	Nano-thermometer	Spectral operation range		Sensitivity (%·°C ⁻¹)	T operation range (°C)	T-sensitive parameter	Ref.
		$\lambda_{\text{excitation}}$ (nm)	$\lambda_{\text{emission}}$ (nm)				
VISIBLE	NaYF ₄ :Er,Yb	920	545, 525	1	20-60	Spectral ratio	[1]
	CaF ₂ :Er,Yb	920	655	1.6	25-50	Spectral ratio	[2]
	CdSe/ZnS QDs	<525	620	0.7	10-80	Intensity	[3]
	Gold Nanoclusters	580	710	0.5	15-45	Fluorescence lifetime	[4]
	Green fluorescent protein	473	530	0.7	20-60	Polarization Anisotropy	[5]
BW-I	CaF ₂ :Tm,Yb	920	790	0.25	25-50	Spectral ratio	[2]
	Y ₂ O ₃ :Yb,Tm	978	815, 656, 460, 454	7.8 max.	-200-27	Spectral ratio	[6]
	Y ₂ O ₃ :Yb,Ho	978	755, 550	9.7 max.	-260-27	Spectral ratio	[6]
	Nd:YAG	808	940	0.15	10-70	Spectral ratio	[7]
	NaYF ₄ :Nd	830	870	0.12	0-150	Spectral ratio	[8]
	LaF ₃ :Nd	808	870	0.1	10-60	Spectral ratio	[9]
	LiLaP ₄ O ₁₂ :Nd,Yb	808	890, 980	0.4	150-600	Spectral ratio	[10]
BW-II	PLGA hybrid nanostructures	808	1064, 1270	2.5	10-55	Spectral ratio	[11]
	LaF ₃ :Nd,Yb	790	1064, 1300	0.1	10-50	Spectral ratio	[12]
	Nd@YbLaF ₃ core/shell NPs	790	1064, 1300	0.41	10-50	Spectral ratio	[12]
	Yb@NdLaF ₃ core/shell NPs	790	1064, 1300	0.36	10-50	Spectral ratio	[12]
	PbS/CdS/ZnS QDs	808	1270	1	10-60	Intensity	This work

Table S1. Properties of different temperature-sensitive fluorescent nanosized systems.

S3. Ex vivo photothermal treatment

Prior to performing in vivo PTT experiments, the possible effect of the prolonged heating on the thermometric capabilities of the QDs were studied ex vivo. For that purpose, a chicken tissue sample was injected with 50 μL of PbS/CdS/ZnS dispersed in PBS (1 mg/mL) and subjected to photothermal heating at a high power density (2 W/cm^2) for two 4-minute-long cycles, during which the emission of the QDs was continuously monitored with an InGaAs camera. Before starting the procedure, as well as after each heating cycle, the laser power was lowered to 0.02 W/cm^2 so that the QD emission was still clearly detectable with the InGaAs camera while no photothermal heating of the sample occurred. The emission intensity of the QDs before, during and after these photothermal treatments is represented in **Figure S2**. It can be clearly seen that the emission intensity of the QDs recovers its baseline room temperature values a few minutes after the end of the photothermal treatment. The intensity oscillations observed after the end of the heating cycle are attributed to oscillations in the laser diode power when the driving current is suddenly reduced down to values close to threshold.

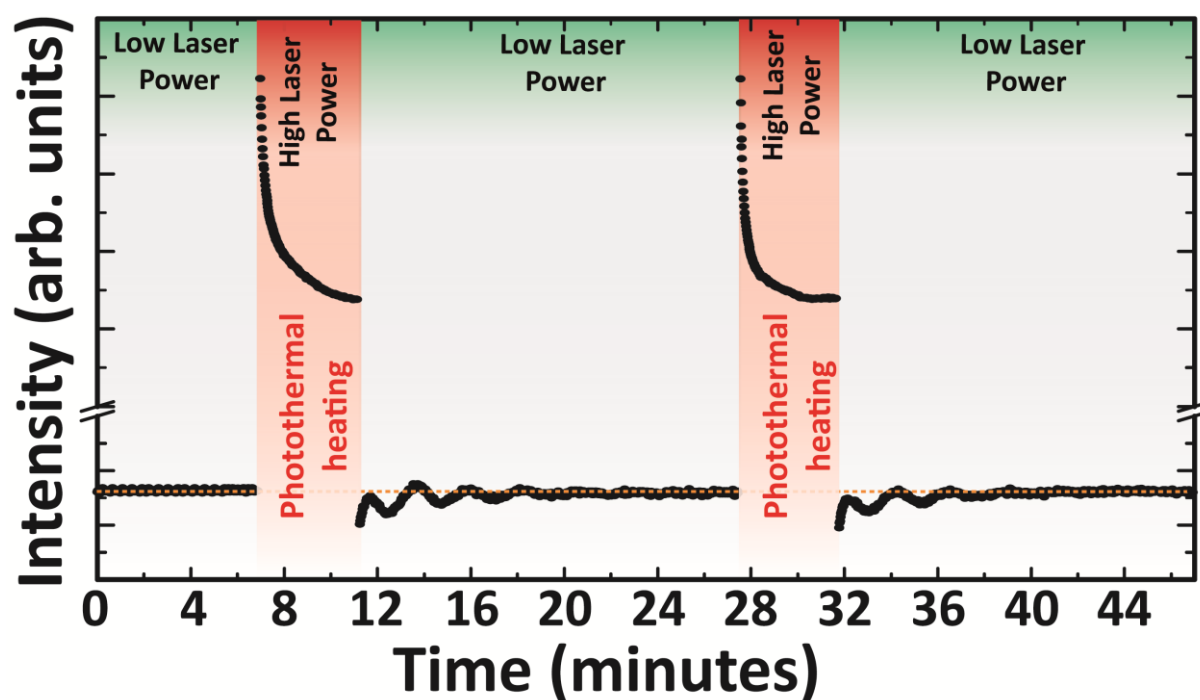


Figure S2. Photothermal heating of an aqueous dispersion of QDs injected ex vivo upon irradiation with an 808 nm laser diode. Before and after the heating, the laser intensity was kept low (0.02 W/cm^2), as labeled in the figure as “Low Laser Power”. During the 4-minute-

long photothermal heating procedures, shadowed in red and labeled as “High Laser Power”, the laser intensity was set to 2 W/cm².

S4. Calculation of the photothermal conversion efficiency of PbS/CdS/ZnS QDs

The photothermal conversion efficiency, η , is defined as the fraction of the absorbed laser energy that is transformed into heat. To calculate the photothermal conversion efficiency of PbS/CdS/ZnS QDs, we followed the method described in different works based on the report presented by Roper et al.^[13] An aqueous dispersion of QDs (1 mg/mL) was placed in an open quartz cuvette and irradiated with an 808 nm laser diode at a power of 403 mW, while continuously monitoring its temperature with a thermographic camera. The laser was turned off when the temperature reached a steady value (18 minutes after starting the irradiation), and the temperature was recorded during the cooling process until the temperature of the dispersion matched that of its surroundings. In figure S1, which contains the experimental data of temperature as a function of time, the heating and cooling periods are indicated.

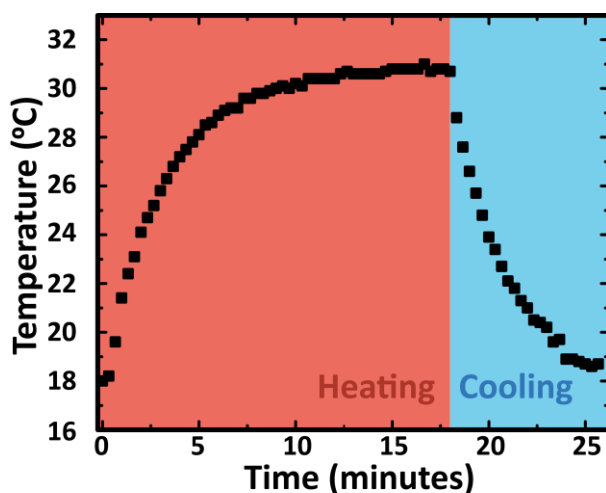


Figure S3. Photothermal heating of an aqueous solution (1 mg/mL) of QDs upon irradiation with 808 nm laser light (403 mW). The laser was kept on for 18 minutes (left part of the figure, shadowed in red) until the temperature of the dispersion had reached a steady value. Then, it was turned off and the temperature was monitored until it was equal to the temperature in the surroundings (right part of the figure, shadowed in blue).

The photothermal conversion efficiency, η , can be defined as follows:

$$\eta = \frac{hA(T_{\max} - T_0) - Q_0}{I(1 - 10^{-OD})} \quad (S1)$$

Where h is the heat transfer coefficient and A , the surface area of the container where the solution is placed, while T_{\max} and T_0 represent the maximum temperature reached by the dispersion containing the QDs and the temperature at the surroundings, respectively. Q_0 corresponds to the heat dissipated from the light absorbed by the solvent and container, I to the laser power and OD to the optical density of the sample.

As explained in the literature, hA can be obtained through the system time constant, τ_s , which can be determined from the cooling curve (see Figure S1), as

$$hA = \frac{m_D C_D}{\tau_s} \quad (\text{S2})$$

where $m_D = 0.5$ g and $C_D = 4.179 \text{ J} \cdot \text{g}^{-1} \cdot \text{s}^{-1}$ correspond to the mass and heat capacity of the solvent, water in our case. Substituting $m_D = 0.5$ g and $C_D = 4.179 \text{ Jg}^{-1}\text{s}^{-1}$ as well as the obtained $\tau_s = 174$ s, we obtain a value of $hA = 12 \text{ mW} \cdot \text{K}^{-1}$.

The maximum temperature increment, $(T_{\max} - T_0)$, as seen in Figure RL1, is 12.8°C for the applied laser power, I , of 403 mW . Q_0 was measured independently using an open quartz cuvette containing distilled water and found to be 38.2 mW . The optical density of the QDs dispersion at this concentration at 808 nm is 0.4746 .

Substituting these numbers into expression (1), we find a laser-to-heat conversion efficiency of 43% .

S5. Comparison of photothermal conversion efficiencies of different nanoheaters

Nanoparticle type	Photothermal conversion efficiency (%)	Irradiation wavelength (nm)	Average NP size (nm)	Ref.
Gold Nanorods	50	808	6.18	[13b]
Gold Nanorods	98.6	808	60.8 x 14.6	[14]
Gold Nanoshells	25	808	145	[13b]
Gold Nanorods and Gold Bipyramids	51-95	809	50 - 10	[15]
Gold Nanospheres	65-80	532	50 - 5	[16]
Gold Nanomatryoshkas	63	810	44	[17]
Porous Pd NPs	93.4	808	22.8	[14]
Polypyrrole (PPy) NPs	44.7	808	50	[18]
PPy-coated Pd NPs	96	808	22	[19]
NaYF ₄ :Yb/Er@PPy core/shell nanoplates	44.7	915	78 x 25	[20]
NaLuF ₄ :Yb,Er@NaLuF ₄ @Carbon	38.1	730	77 (hydrodynamic diameter)	[21]
Iridium complex loaded PPy NPs	35.5	730	60	[22]
PEG-MoO _{3-x} Hollow Nanospheres	22.64	808	90	[23]
PEG-Sb nanorods	41	808	200-300 long 10 thick	33
Dopamin-melanin Colloidal Nanospheres	40	808	160	[24]
NdVO ₄ NPs	57.9	808	2.6	
Cys-CuS	27	980	18	[25]
Cu _{7.2} S ₄ Nanocrystals	56.7	980	20	[26]
Cu ₃ BiS ₃ Hollow Nanospheres	27.5	980	80	[27]
MoSe ₂ nanodots	46.5	785	2-3	[28]
CdSe/Bi ₂ Se ₃ QDs	27.1	808	5	[29]
WS ₂ QDs	44.3	808	3	[30]

Table S2. Photothermal conversion efficiencies of different nanosized systems with remarkable laser-to-heat conversion capabilities. In the cases where multiple values are reported for the same NP type (gold nanorods/bipyramids and gold nanospheres), the authors report on an increased photothermal conversion efficiency for smaller nanoparticles.

S6. In vitro toxicity of PbS/CdS/ZnS after heating

This study was undertaken using a cervical cancer cell line, HeLa. Cells were routinely cultivated using Dulbecco modified Eagle medium (DMEM) containing 10% (vol/vol) fetal calf serum (FCS), 50 units/mL penicillin, 50 µg/mL streptomycin. Cell cultures were performed at 37 °C in a humidified atmosphere containing 5% CO₂.

The MTT (3-(4,5-dimethylthiazol-2-yl)-2,5-diphenyltetrazolium bromide) assay is a simple non-radioactive colorimetric assay to measure cell cytotoxicity, proliferation or viability.

MTT is yellow, water soluble, tetrazolium salt. Metabolically active cells are able to convert this dye into a water-insoluble dark blue formazan by reductive cleavage of the tetrazolium ring. Formazan crystals, then, can be dissolved in an organic solvent such as dimethylsulphoxide (DMSO) and quantified by measuring the absorbance of the solution at 540 nm, and the resultant value is related to the number of living cells. To determine cell cytotoxicity/viability, the cells were plated in a 24 well plate at 37 °C in 5% CO₂ atmosphere. After 48 h of culture, the medium in the well was replaced with the fresh medium containing QDs, previously heated or not (see **Figure S4**) and cells were incubated for 2, 4, 6 and 8 hours. After incubation, the medium was removed and changed to medium without QDs. After 24 h, 0.5 mL of MTT dye solution (0.05 mg/mL of MTT, Sigma) was added to each well. After 2-3 h of incubation at 37 °C and 5% CO₂, the medium was removed and formazan crystals were solubilized with 0.5 mL of DMSO and the solution was vigorously mixed to dissolve the reacted dye. The absorbance of each well was read on a microplate reader at 540 nm. The relative cell viability (%) related to control wells containing cell culture medium without QDs was calculated according to:

$$\text{Viability} = \frac{[A]_{\text{test}}}{[A]_{\text{control}}} \times 100 \quad (\text{S3})$$

Where $[A]_{\text{test}}$ and $[A]_{\text{control}}$ correspond to the absorbance of the test and control samples, respectively.

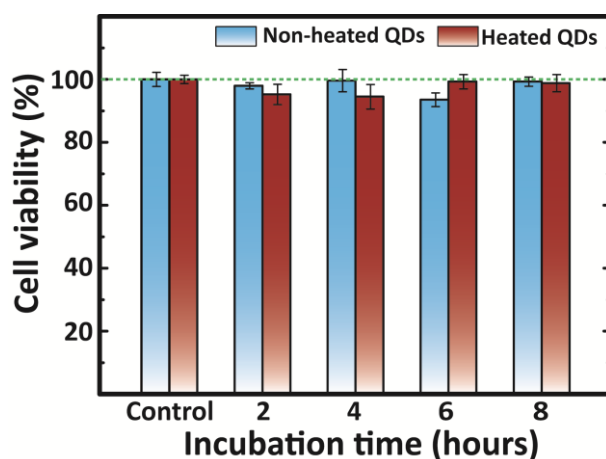


Figure S4. Cell viability of HeLa cancer cells after incubation with a dispersion of PbS/CdS/ZnS QDs in PBS at a concentration of 40 $\mu\text{g/mL}$ for different incubation times. The red bars correspond to QDs that had been previously subjected to a heating procedure (up to 80 $^{\circ}\text{C}$ for 4 minutes), while the blue bars correspond to QDs that had not been previously heated. Each bar corresponds to the mean cell viability value \pm standard deviation.

S7. Comparison of surface temperatures achieved in PTT experiments

Nanoparticle type	Irradiation parameters			Surface maximum temperature (°C)		Ref.
	λ (nm)	time (min)	Power density (W/cm ²)	Treated	Control	
SWCNTs	808	5	0.6	60	45	[31]
Graphene NPs	808	5	0.15	48	38	[32]
GNRs	810	3	2	75	40	[33]
Sb NPs	808	5	1	55	37	[34]
FeS nanoplates	808	5	1	60	45	[35]
LaF₃:Nd	808	4	4	48	41	[36]
MoS₂-iron oxide	808	5	0.78	51	40	[37]
Mn-iron oxide	808	5	1.5	70	43	[38]
WS₂ QDs	808	10	1	~45	38	[30]

Table S3. Treatment conditions (irradiation wavelength, duration and power density) and surface maximum temperatures for different PTT experiments in animal models. In all cases, the surface maximum temperature in the successfully treated tumors and in the laser-only control cases were measured using thermographic imaging.

REFERENCES

- [1] F. Vetrone, R. Naccache, A. Zamarron, A. Juarranz de la Fuente, F. Sanz-Rodriguez, L. Martinez Maestro, E. Martin Rodriguez, D. Jaque, J. Garcia Sole, J. A. Capobianco, *ACS Nano* **2010**, *4*, 3254.
- [2] N. Dong, M. Pedroni, F. Piccinelli, G. Conti, A. Sbarbati, J. R. Hernandez, L. M. Maestro, M. C. Iglesias de la Cruz, F. Sanz-Rodriguez, A. Juarranz, *Acs Nano* **2011**.
- [3] B. Han, W. L. Hanson, K. Bensalah, A. Tuncel, J. M. Stern, J. A. Cadeddu, *Annals of Biomedical Engineering* **2009**, *37*, 1230.
- [4] L. Shang, F. Stockmar, N. Azadfar, G. U. Nienhaus, *Angew. Chem., Int. Ed.* **2013**, *52*, 11154.
- [5] J. S. Donner, S. A. Thompson, M. P. Kreuzer, G. Baffou, R. Quidant, *Nano Lett.* **2012**, *12*, 2107.
- [6] V. Lojpur, M. Nikolic, L. Mancic, O. Milosevic, M. Dramicanin, *Ceramics International* **2013**, *39*, 1129.
- [7] A. Benayas, B. del Rosal, A. Pérez-Delgado, K. Santacruz-Gómez, D. Jaque, G. A. Hirata, F. Vetrone, *Adv. Opt. Mater.* **2015**, *3*, 687.
- [8] D. Wawrzynczyk, A. Bednarkiewicz, M. Nyk, W. Strek, M. Samoc, *Nanoscale* **2012**, *4*, 6959.
- [9] U. Rocha, C. Jacinto da Silva, W. Ferreira Silva, I. Guedes, A. Benayas, L. Martínez Maestro, M. Acosta Elias, E. Bovero, F. C. J. M. van Veggel, J. A. García Solé, D. Jaque, *ACS Nano* **2013**, *7*, 1188.
- [10] L. Marciniak, A. Bednarkiewicz, M. Stefanski, R. Tomala, D. Hreniak, W. Strek, *Phys. Chem. Chem. Phys.* **2015**, *17*, 24315.
- [11] E. N. Cerón, D. H. Ortgies, B. del Rosal, F. Ren, A. Benayas, F. Vetrone, D. Ma, F. Sanz-Rodríguez, J. G. Solé, D. Jaque, E. M. Rodríguez, *Adv. Mater.* **2015**, *27*, 4781.
- [12] E. C. Ximendes, U. Rocha, C. Jacinto, K. U. Kumar, D. Bravo, F. J. Lopez, E. M. Rodriguez, J. Garcia-Sole, D. Jaque, *Nanoscale* **2016**, *8*, 3057.
- [13] a) Q. Tian, F. Jiang, R. Zou, Q. Liu, Z. Chen, M. Zhu, S. Yang, J. Wang, J. Wang, J. Hu, *ACS Nano* **2011**, *5*, 9761; b) V. P. Pattani, J. W. Tunnell, *Lasers in Surgery and Medicine* **2012**, *44*, 675; c) D. K. Roper, W. Ahn, M. Hoepfner, *The Journal of Physical Chemistry C* **2007**, *111*, 3636.
- [14] J.-W. Xiao, S.-X. Fan, F. Wang, L.-D. Sun, X.-Y. Zheng, C.-H. Yan, *Nanoscale* **2014**, *6*, 4345.
- [15] H. Chen, L. Shao, T. Ming, Z. Sun, C. Zhao, B. Yang, J. Wang, *Small* **2010**, *6*, 2272.
- [16] K. Jiang, D. A. Smith, A. Pinchuk, *The Journal of Physical Chemistry C* **2013**, *117*, 27073.
- [17] C. Ayala-Orozco, C. Urban, M. W. Knight, A. S. Urban, O. Neumann, S. W. Bishnoi, S. Mukherjee, A. M. Goodman, H. Charron, T. Mitchell, M. Shea, R. Roy, S. Nanda, R. Schiff, N. J. Halas, A. Joshi, *ACS Nano* **2014**, *8*, 6372.
- [18] M. Chen, X. Fang, S. Tang, N. Zheng, *Chem. Commun.* **2012**, *48*, 8934.
- [19] Y. Liu, D.-D. Wang, L. Zhao, M. Lin, H.-Z. Sun, H.-C. Sun, B. Yang, *RSC Advances* **2016**, *6*, 15854.
- [20] X. Huang, B. Li, C. Peng, G. Song, Y. Peng, Z. Xiao, X. Liu, J. Yang, L. Yu, J. Hu, *Nanoscale* **2016**, *8*, 1040.
- [21] X. Zhu, W. Feng, J. Chang, Y.-W. Tan, J. Li, M. Chen, Y. Sun, F. Li, *Nat. Commun.* **2016**, *7*.
- [22] F. Xue, M. Shi, Y. Yan, H. Yang, Z. Zhou, S. Yang, *RSC Advances* **2016**, *6*, 15509.

- [23] T. Bao, W. Yin, X. Zheng, X. Zhang, J. Yu, X. Dong, Y. Yong, F. Gao, L. Yan, Z. Gu, Y. Zhao, *Biomaterials* **2016**, 76, 11.
- [24] Y. Liu, K. Ai, J. Liu, M. Deng, Y. He, L. Lu, *Adv. Mater.* **2013**, 25, 1353.
- [25] X. Liu, B. Li, F. Fu, K. Xu, R. Zou, Q. Wang, B. Zhang, Z. Chen, J. Hu, *Dalton Trans.* **2014**, 43, 11709.
- [26] B. Li, Q. Wang, R. Zou, X. Liu, K. Xu, W. Li, J. Hu, *Nanoscale* **2014**, 6, 3274.
- [27] S.-M. Zhou, D.-K. Ma, S.-H. Zhang, W. Wang, W. Chen, S.-M. Huang, K. Yu, *Nanoscale* **2016**, 8, 1374.
- [28] L. Yuwen, J. Zhou, Y. Zhang, Q. Zhang, J. Shan, Z. Luo, L. Weng, Z. Teng, L. Wang, *Nanoscale* **2016**.
- [29] G. Z. Jia, W. K. Lou, F. Cheng, X. L. Wang, J. H. Yao, N. Dai, H. Q. Lin, K. Chang, *Nano Res.* **2015**, 8, 1443.
- [30] Y. Yong, X. Cheng, T. Bao, M. Zu, L. Yan, W. Yin, C. Ge, D. Wang, Z. Gu, Y. Zhao, *ACS Nano* **2015**, 9, 12451.
- [31] J. T. Robinson, K. Welsher, S. M. Tabakman, S. P. Sherlock, H. Wang, R. Luong, H. Dai, *Nano Res.* **2010**, 3, 779.
- [32] K. Yang, J. Wan, S. Zhang, B. Tian, Y. Zhang, Z. Liu, *Biomaterials* **2012**, 33, 2206.
- [33] G. von Maltzahn, A. Centrone, J.-H. Park, R. Ramanathan, M. J. Sailor, T. A. Hatton, S. N. Bhatia, *Adv. Mater.* **2009**, 21, 3175.
- [34] W. Li, P. Rong, K. Yang, P. Huang, K. Sun, X. Chen, *Biomaterials* **2015**, 45, 18.
- [35] K. Yang, G. Yang, L. Chen, L. Cheng, L. Wang, C. Ge, Z. Liu, *Biomaterials* **2015**, 38, 1.
- [36] E. Carrasco, B. del Rosal, F. Sanz-Rodríguez, Á. J. de la Fuente, P. H. Gonzalez, U. Rocha, K. U. Kumar, C. Jacinto, J. G. Solé, D. Jaque, *Adv. Funct. Mater.* **2015**, 25, 615.
- [37] T. Liu, S. Shi, C. Liang, S. Shen, L. Cheng, C. Wang, X. Song, S. Goel, T. E. Barnhart, W. Cai, Z. Liu, *ACS Nano* **2015**, 9, 950.
- [38] M. Zhang, Y. Cao, L. Wang, Y. Ma, X. Tu, Z. Zhang, *ACS Applied Materials & Interfaces* **2015**, 7, 4650.